

Reflection halo twins: subsun and supersun

Gunther P. Können^{1,*} and Siebren Y. van der Werf²

¹Sophialaan 4, NL-3761DK Soest, The Netherlands

²Kernfysisch Versneller Instituut, University of Groningen, Zernikelaan 25, NL-9747 AA Groningen, The Netherlands

*Corresponding author: konnen@planet.nl

Received 2 May 2011; revised 27 July 2011; accepted 31 July 2011;
posted 1 August 2011 (Doc. ID 146958); published 21 September 2011

From an aircraft, a short distinct vertical structure is sometimes seen above the setting sun. Such a feature can be understood as a halo, which is the counterpart of the well-known subsun. Whereas the latter arises from reflections off basal faces of plate-oriented ice crystals illuminated from above, what we call the supersun emerges when these crystals are illuminated from below. The supersun occurs when the sun is below the true horizon and is only visible from elevated positions. The curvature of the Earth causes the ensemble of reflecting crystal faces to act as a hollow mirror and the supersun appears as a vertical band of uniform width, extending from the sun upwards to its supersolar point. We discuss the geometrical properties of the phenomenon and simulate its shape and radiance distribution with an extended version of an atmospheric ray-tracing program. © 2011 Optical Society of America

OCIS codes: 010.2940, 010.1290, 010.1310, 290.5850.

1. Introduction

Figure 1 shows what on first inspection resembles a vertically elongated mirror image of the sun, with its center at $2^\circ.1$ above the upper rim of the setting sun. The phenomenon appeared during a 1 h 50 min flight from Oslo to Kirkenes, in the far northeast of Norway ($69^\circ46'N$, $30^\circ5'E$), on 10 September 2008. Takeoff was at 16:30 UTC; 1 hour later the aircraft flew through a cold front whose clouds extended to the level of the aircraft. Just before the aircraft entered the clear sky behind the front, a bright parhelion appeared (Fig. 2), proving the presence of plate-oriented ice crystals in the frontal clouds. Sunset, 75 min after takeoff and 15 min after the frontal passage, took place in the receding cloud layer of the just-passed front, which by then was 150 km away. The apparent angular height of the frontal cloud layer was estimated from the photo to be $3^\circ.2$, in accordance with the value of the horizon dip of $3^\circ.3$ for 12 km altitude. Two pictures of the setting sun with the feature above it were taken. From these, the width of the spot was found to be $0^\circ.5$, equal to the

sun's diameter within the uncertainty. The spot's vertical dimension was $0^\circ.8$; it extended from $1^\circ.8$ to $2^\circ.6$ above the upper limb of the sun, which was about $0^\circ.1$ above the apparent horizon, the latter being by definition the direction in which the edge between sea and sky is seen from an elevated position. Closer inspection of Fig. 1 reveals that an upward extension of the spot is still perceptible up to the top of the cloud layer.

Despite the elongated shape, the observed feature does not seem to be an ordinary pillar and our attempts to simulate it as such with Cowley and Schroeder's HaloSim program [1] failed to adequately reproduce its distinct shape and uniform width.

We interpret this feature as due to the reflection of sunlight from the horizontally oriented faces of plate-oriented airborne ice crystals, just like in the case of the subsun. With the sun below the true horizon (i.e., the locally horizontal direction), even a perfectly horizontal crystal face can be illuminated from below, which creates a mirror image above the sun. The image of the resulting halo is, however, not a simple inversion of that of the subsun: due to the curvature of the Earth, the reflecting basal faces of distant plate-oriented crystals are not parallel with

0003-6935/11/280F80-09\$15.00/0
© 2011 Optical Society of America



Fig. 1. (Color online) Vertically elongated structure above the sun. It extends upwards to $2^{\circ}.6$ above the sun and has a width of $0^{\circ}.5$. The sun is setting behind the apparent horizon, which is $3^{\circ}.3$ below the true horizon. The horizontal field of view of the picture is 13° . Photograph taken on 10 September 2008 at 17:46 UTC by G.P. Können on a flight from Oslo to Kirkenes (Norway) from a height of 12 km.

the aircraft's horizontal, but instead with respect to their own local horizontals. In this scattering geometry, the Spin Vector Assumption [2,3] is not satisfied in the line of sight of the observer and the ensemble of crystal basal faces acts as a hollow fun house mirror, causing the reflected image to appear as a distinct vertical band of uniform width extending upwards to the supersolar point—which is the point directly above the sun, equally high above the aircraft's true horizon as the sun is below it.

To our knowledge, the effect of the Earth's roundness on the appearance of near-horizon halos or near-horizon halo segments has not been discussed before. The above-mentioned observation inspired us to do a quantitative analysis of the shape and radiance

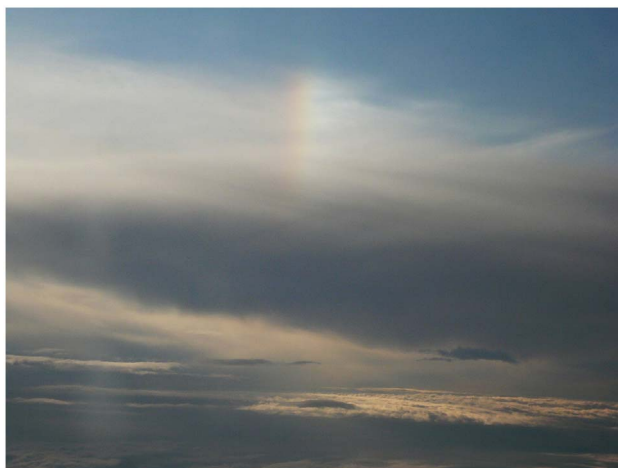


Fig. 2. (Color online) Parhelion, photographed during the passage through the frontal clouds. The appearance of this halo proves that horizontally oriented crystal faces were present in the frontal clouds in which the vertical feature of Fig. 1 appeared 14 min later. The horizontal field of view of the picture is 21° . Photograph taken on 10 September 2008 at 17:32 UTC by G.P. Können.

distributions of halos due to reflection at horizontally oriented crystal faces for the sun on either side of the horizontal. For positive solar altitudes and a flat Earth, this halo appears as the reflection of the sun's image across the horizontal and is known as the sub-sun. Traditionally, the term “subsun” refers to the situation where the sun is above the horizontal, but due to the Earth's curvature this reflection halo can also develop below the sun when the latter is below the horizontal but still visible above a dipped horizon. To avoid proliferation of terminology, we will call this extension by the same name: the subsun. Emphasis, however, in the present paper will be on the feature that develops above the sun for negative sun altitudes. It can be regarded as a deformed counterpart of the usual subsun, and we will name it by its corresponding Latin prefix: the supersun [4].

2. Geometry of Subsun/Supersun Formation for a Round Earth

A. General Considerations

The geometry of the problem is depicted in Fig. 3. R_{aircraft} and R_{xtl} are the distances to the Earth's center of the aircraft and of the reflecting crystal, respectively. α and β are the sun's depression angles as seen from the aircraft and from the reflecting crystal: the sun's angular distance below the true horizon of these respective locations. At the same time, α is the angular distance between the aircraft's geographical position and the terminator of the Earth, which is positive when the sun is below the horizontal. Likewise, β is the angular distance between the reflecting crystal and the terminator. The angle γ , which measures the angular distance between the geographical positions of the aircraft and the reflecting crystal, equals the tilt angle of the reflecting crystal basal face with respect to the aircraft's true horizontal. γ is always

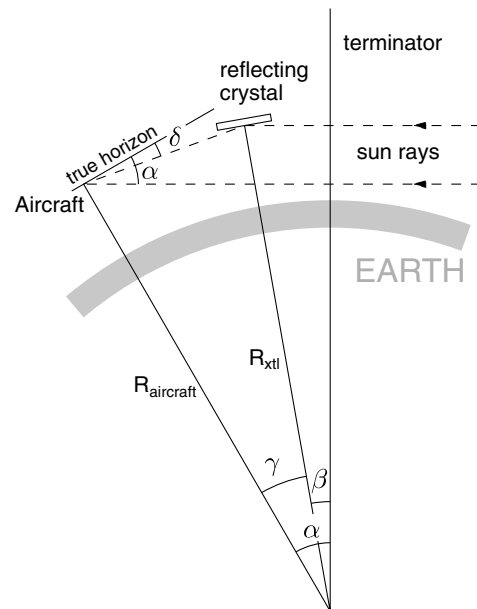


Fig. 3. Geometry of supersun formation by reflection of crystals at a negative sun altitude.

positive. From the aircraft, the reflecting crystal is viewed at a (positive or negative) depression angle δ . For the observer, the crystal creates a light point on the celestial sphere, called a halo point [2]; the total of the halo points of all reflecting crystals makes up the halo. For the moment, we ignore the effect of refraction and consider the rays as perfectly straight lines. Inspection of Fig. 3 shows

$$\beta = \alpha - \gamma \quad (1)$$

and

$$\delta = \alpha - 2\beta = -\alpha + 2\gamma \quad (2)$$

and

$$R_{\text{xtl}} = R_{\text{aircraft}} \frac{\cos(\delta)}{\cos(\beta)} = R_{\text{aircraft}} \frac{\cos(\alpha - 2\gamma)}{\cos(\alpha - \gamma)}. \quad (3)$$

We insert in this expression $h_{\text{xtl}} \equiv R_{\text{xtl}} - R_{\text{Earth}}$, being the height of the reflecting crystal above the Earth, and $h_0 \equiv R_{\text{aircraft}} - R_{\text{Earth}}$, the height of the aircraft above the Earth—also called the flight level of the aircraft. Then Eq. (3) modifies to

$$h_{\text{xtl}}(\gamma) = h_0 - 2R_{\text{aircraft}} \frac{\cos(\frac{1}{2}\gamma) \sin[\frac{1}{2}(2\alpha - 3\gamma)]}{\cos(\alpha - \gamma)}. \quad (4)$$

For a fixed solar depression angle, α , Eq. (3) gives the general expression for the locus of the reflecting crystals, which contribute to the image the observer gets to see. It is valid for negative ($\alpha > 0$) as well as for positive ($\alpha < 0$) sun altitudes. Equation (3) shows that the locus starts (at $\gamma = 0$) at the aircraft's flight level, where the reflecting crystals surrounding the aircraft create a halo point at the subsolar (for $\alpha < 0$) or supersolar point (for $\alpha > 0$). Equation (4) shows that the height of the locus above the aircraft's flight level, $h_{\text{xtl}}(\gamma) - h_0$, is virtually independent of h_0 , as R_{aircraft} equals R_{Earth} , the radius of the Earth, within 0.02%. Figure 4 illustrates how, for a negative sun altitude, the part of the locus above the night side of the Earth produces a supersun and the part above the daylight side a subsun. As already mentioned in Section 1, the roundness of the Earth extends the regime of sun altitudes where the subsun may occur all the way down to the observer's dipped horizon. Figure 4 shows how, for negative sun heights but still above the apparent horizon, the supersun and the subsun may both be seen at the same time—where visually the latter appears as the downward continuation of the former.

According to Eq. (3), the locus would extend all the way down from the aircraft's position ($\gamma = 0$) to the center of the Earth ($\delta = 90^\circ$, or $\gamma = 45^\circ + \alpha/2$). But obviously only the part of the locus above the Earth's surface contributes. This sets an upper limit on γ , which is found by putting h_{xtl} equal to zero in Eq. (4).

Supersun-creating sun rays all have to travel past the terminator before they hit a crystal. They reach their minimum distance from the Earth's center,

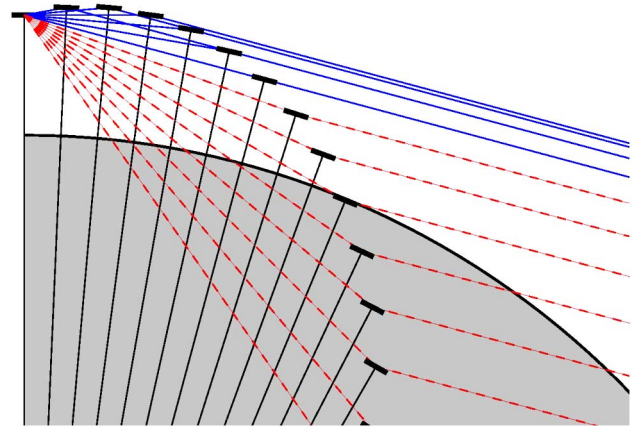


Fig. 4. (Color online) Locus of the positions of reflecting horizontal faces creating the subsun/supersun. The figure is for a sun below the true horizon, but above the apparent horizon. Blue (solid) rays reflect from bottom faces, red (dashed) rays from top faces. In the former case, the distance of the locus above the Earth shows a local maximum. To the right, the surface of the Earth puts a lower bound on the subsun.

R_{min} , straight over the terminator (see Fig. 3). From the figure and Eq. (3), it follows that R_{min} is given by

$$R_{\text{min}} = R_{\text{aircraft}} \cos(\delta), \quad (5)$$

so that $R_{\text{min}} < R_{\text{aircraft}}$ for any $\delta \neq 0$. This implies that for a ground-based observer ($R_{\text{aircraft}} = R_{\text{Earth}}$) all supersun-making sun rays are blocked by the Earth. Consequently, a supersun or a segment of it can only be observed by an observer flying in the air or standing at an elevated position.

Table 1 lists five special points on the locus together with their numerical values for $\alpha = 3^\circ.2$, corresponding to the situation as photographed (Fig. 1). The first of these points is $\gamma = 0$, which is the observer's position, where the ice crystals immediately in front of him create the supersun's upper edge. The last of the five points is $\gamma = \alpha$, which corresponds to the lower edge of the supersun. Halfway between aircraft and terminator, at $\gamma = \frac{1}{2}\alpha$, the contributing crystals are viewed on the observer's true horizon. The locus reaches its highest point above the aircraft's flight level for $\gamma = \frac{1}{3}\alpha$ and crosses the flight level again at $\gamma = \frac{2}{3}\alpha$. Because an aircraft's typical cruise altitude (≈ 12 km) is usually well above the cloud tops, the most relevant region of γ is the interval $[\frac{2}{3}\alpha, \alpha]$, where the reflected light comes from crystals floating below the aircraft's flight level. This segment of the supersun, which is still entirely below the true horizon, is what is most often observable for an air passenger.

B. Restrictions on the Supersun's Appearance

A first restriction applies to the sun altitude. A supersun can only appear when the crystals are illuminated from below. Since angles are counted as positive from the true horizon downward in Fig. 3, this condition means $\beta > 0$, or, by Eq. (1), that $\gamma < \alpha$. As γ is always counted positive in the observer's

Table 1. Special Points on the Reflection Locus for Sun Depression $\alpha = 3^\circ.2^a$

Angular Distance Aircraft–Crystal	Horizontal Distance Aircraft–Crystal	Height of the Reflecting Crystals Above the Aircraft’s Flight Level	Angular Distance Halo Point Above the Aircraft’s Horizon (= $-\delta$)	Characteristic
$\gamma = 0$	0 km	0 km	$+3^\circ.2^b$	crystals near the observer; $\delta = -\alpha$
$\gamma = \frac{1}{3}\alpha$	118 km	$+3.3 \text{ km}^b$	$+1^\circ.1$	top of locus
$\gamma = \frac{2}{3}\alpha$	178 km	$+2.5 \text{ km}$	0°	$\delta = 0^\circ$
$\gamma = \frac{2}{3}\alpha$	237 km	0 km	$-1^\circ.1$	crystals at aircraft’s flight level
$\gamma = \alpha$	355 km	-9.9 km	$-3^\circ.2$	crystals above the terminator; $\delta = \alpha$

^aSun taken as a point source. As in Eqs. (1)–(4) and (6), on which this table is based, refraction is ignored.

^bMaximum values.

viewing direction, this situation can only occur when $\alpha > 0$, a positive solar depression angle, hence a negative sun altitude. Conversely, when the sun has a positive altitude ($\alpha < 0$), a subsun may be seen via reflections off the top faces of the crystals, described by $\beta < 0$.

A second restriction applies to the length of the supersun. From Eq. (2) follows that the supersun extends from the direct image of the sun, where $\beta = 0$, hence $\delta = \alpha$, upwards to the supersolar point, a distance of 2α above it that corresponds to reflections immediately in front of the observer: $\gamma = 0$, where $\delta = -\alpha$. This restriction applies as long as the sun is seen above the apparent horizon. For an aircraft at 12 km height, the horizon dip amounts to $3^\circ 31'$ without refraction, or $3^\circ 19'$ when atmospheric refraction is included. When the sun is below the apparent horizon, $\alpha > \text{dip}$ and the supersun is naturally seen only from the apparent horizon upwards. It can easily be understood that it is then also cut off from above at a height that corresponds to the “mirror horizon,” that is, a distance equal to the dip above the true horizon.

A third restriction is introduced when the presence of ice crystals is limited to a certain region between a lower and an upper height above the ground. Writing as before $h_{\text{xtl}} \equiv R_{\text{xtl}} - R_{\text{Earth}}$ and $h_0 \equiv R_{\text{aircraft}} - R_{\text{Earth}}$, Eq. (4) gives to leading order

$$\gamma(2\alpha - 3\gamma) = \left(\frac{\delta + \alpha}{2}\right)\left(\frac{\alpha - 3\delta}{2}\right) \approx \frac{2(h_{\text{xtl}} - h_0)}{R_{\text{Earth}}}, \quad (6)$$

which is rewritten as

$$\alpha = \delta \pm \sqrt{\delta^2 + 2(h_{\text{xtl}} - h_0)/R_{\text{Earth}}}. \quad (7)$$

This is a hyperbola in the plane of δ versus α , whose shape depends on the crystal height minus the aircraft height, $h_{\text{xtl}} - h_0$.

C. Ray Tracing

These three geometrical restrictions on the image of the supersun, and at the same time that of the subsun, are illustrated by a ray tracing calculation (Fig. 5).

From the position of the observer, 12 km above the Earth, rays are followed to the right. The

procedure has been described in earlier publications [5–7]. Consistent with the foregoing discussion, we neglect refraction for the moment. The integration is done by path length, as described in [7], and after each integration step a random number $\text{rnd}(1)$ from a uniform distribution between 0 and 1, is generated to decide whether or not to attribute a reflection to the ray at that point.

The probability of a reflection taking place must scale with the area that the crystal presents at right angles with the incoming ray. The observer views the crystal under an angle β , as defined in Fig. 3. Accordingly, we adopt the criterion

$$\begin{aligned} \text{rnd}(1) |\sin(\beta)| < ds/\lambda_0 &\rightarrow \text{reflection,} \\ \text{rnd}(1) |\sin(\beta)| \geq ds/\lambda_0 &\rightarrow \text{no reflection,} \end{aligned} \quad (8)$$

where ds is the integration step size and λ_0 defines a mean free path length.

Rays are calculated for observed angles from -15° to $+15^\circ$ in steps of $0'.01$. The mean free path is adjusted such that the number of rays with 0, 1, 2, ... reflections decreases by about a factor of 10 for each additional reflection. On a fundamental note, including reflections of all orders and *a posteriori* selecting the ensemble of single reflections respects time reversal invariance and therewith the procedure of doing ray tracing backwards. A forced limitation to zero or one reflections, on the other

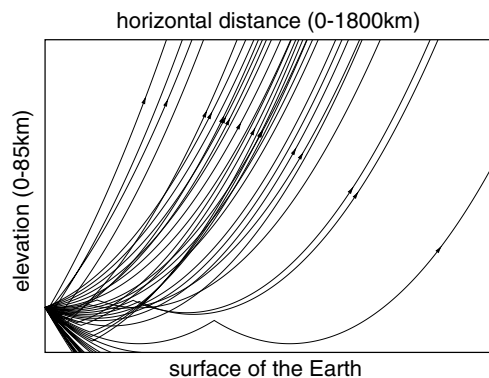


Fig. 5. Ray tracing for subsun/supersun simulation. The rays are traced backward from the observer until they reach the upper mesosphere. Because the Earth’s surface is drawn as a straight line, all light rays bend upward. A kink indicates the place where a ray is reflected by a horizontally oriented crystal face.

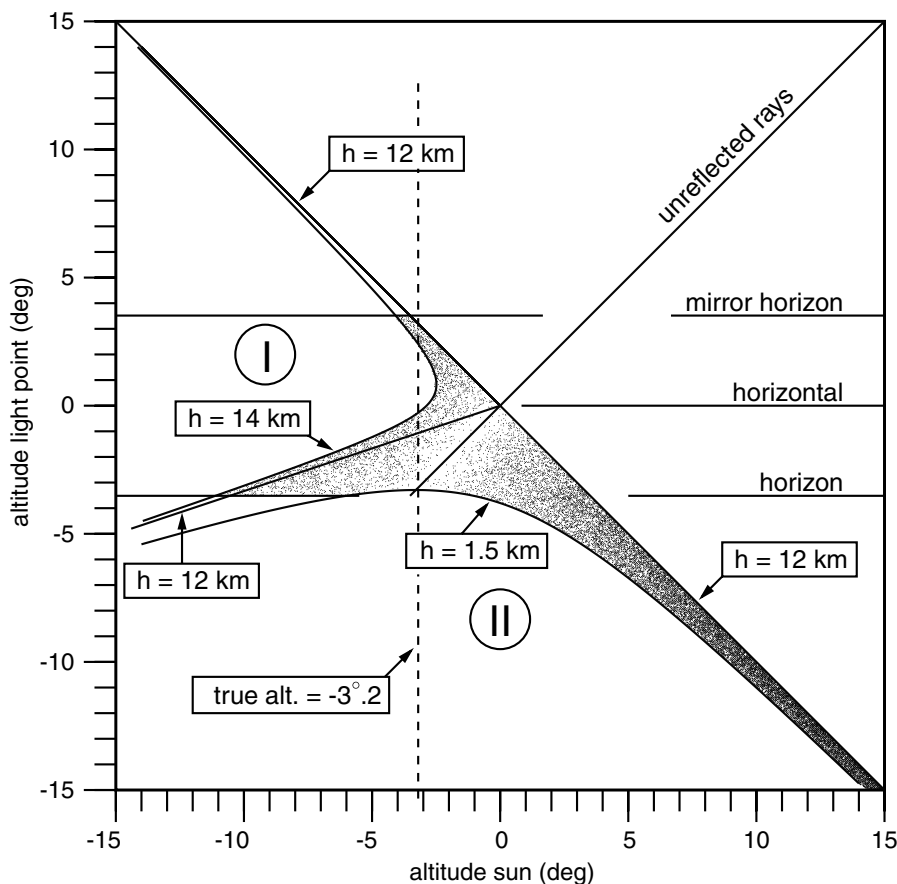


Fig. 6. Scatter plot and limits on the subsun and supersun for a single reflection off horizontally oriented faces of ice crystals, assumed present between 1.5 and 14 km above the Earth's surface. Atmospheric refraction is neglected; the sun is taken as a point source. Points above the diagonal contribute to the supersun, those below it to the subsun. The dashed vertical line indicates a sun altitude of $-3^\circ.2$. The aircraft is at 12 km above the Earth, and, in the absence of refraction, horizon dip = $3^\circ.5$.

hand, would make the single-reflection ensembles differ for forward and backward ray tracing.

The scatter plot of single reflections is shown in Fig. 6. It constitutes a cloud of points in the plane of the observed altitude of the light points ($-\delta$) versus the altitude of the sun ($-\alpha$), taken as a point source. The subsun and the supersun, though described by the same mathematical form of their locus, are distinct phenomena and the density of the points drops to zero on both sides of the diagonal line that separates them.

The three restrictions formulated above appear naturally:

1. For small solar depression angles, the supersun ranges from the sun itself, on the diagonal, to the antidiagonal, which is its mirror across the true horizontal.
2. For larger depression angles, the supersun is cut off at the apparent horizon on its lower side and by the mirror horizon from above.
3. The limits imposed by the height of the crystals as found from Eq. (7) show up as hyperbolic curves. The upper limit is taken here as 14 km above the Earth and the corresponding hyperbola lies in the sector to the left, indicated by I. The lower limit

for the ice crystals is taken as 1.5 km, and produces a hyperbola in sector II. The latter limits the scatter plot both for the supersun and the subsun. For $h = h_0 = 12$ km, both hyperbola's have shrunk to their asymptotic lines, showing once more that the antidiagonal itself bounds the scatter plot.

An additional restriction arises when the front of the ice crystals begins at some distance away from the observer. In that case, an additional region below the antidiagonal and parallel to it is blanked out. This has not been indicated in Fig. 6.

The dashed vertical line in Fig. 6 indicates the altitude of the sun as it was in the situation when the photograph in Fig. 1 was taken. This is the region where the locus [Eq. (3)] rises above the adopted limit of 14 km; see also Table 1. As a consequence, the supersun shows itself in two parts, with a darker zone in between.

3. Radiance Distributions of the Subsun and the Supersun

A realistic ray-tracing analysis of near-horizon phenomena must include atmospheric refraction, loss of intensity by reflections off the ice crystals, and atmospheric extinction. We chose the US1976

standard atmosphere [8] and performed the analysis as described above, by calculating rays for apparent altitudes between -15° and $+15^\circ$ in steps of $0'.01$. Refraction and air mass are calculated as path integrals [7] and stored, after which a (true) sun altitude can be chosen and those rays selected that happen to hit the sun disk on their outgoing path.

A. Refraction and Geometry

Atmospheric refraction makes the horizon dip as seen from the 12 km flight level decrease from $3^\circ 31'$ to $3^\circ 19'$. At the horizon, refraction for unreflected rays amounts to $62'$, and the true altitude is $-4^\circ 21'$. The diagonal in Fig. 6, which is the locus of the direct sun in this figure, gets a little curved just above the horizon and the same curvature shows up in the anti-diagonal, which is its mirrored shape. Also, the boundaries imposed by restricting the ice crystals to a height interval between 1.5 and 14 km are no longer the perfect hyperbolas of Eq. (7), but still resemble them closely.

All geometric considerations of the previous section remain valid and the resulting shape of the scatter plot for single reflections closely resembles that of Fig. 6.

B. Intensity Loss at Reflection

Reflections from horizontally oriented crystal faces occur in the ray-tracing calculation via the randomization procedure described in Section 2. For each such reflection, the Fresnel coefficient for external reflection, \mathcal{R} , is evaluated. Light may, however, also be reflected under the same angle via one or more internal reflections within a crystal. In Tape's notation [9], this may occur via ray paths 326 and 316 for the subsun and the supersun, respectively. These internal reflection modes add to the external reflection and an appropriate estimate for the total reflectance is $\frac{1}{2}(1 + \mathcal{R})$, rather than \mathcal{R} . The effect of this replacement is, however, small: in the range of sun altitudes studied here, the crystals' tilt angles are always small enough to make $\mathcal{R} > 0.8$, hence $\frac{1}{2}(1 + \mathcal{R}) > 0.9$.

C. Atmospheric Extinction

The radiance or brightness of the supersun scales with a geometric factor $\sin(\beta)$ and with the total reflectance. In addition, the radiance distribution is affected by extinction and the latter is found to be the governing factor. The reason is that within its angular range from the subhorizontal sun to its supersolar point, the path length of the rays through the atmosphere varies in an extremely drastic manner.

Extinction may be described by the Lambert–Beer law as

$$\ln(I) - \ln(I_0) = -bX/X_0, \quad (9)$$

where X is the air mass along the light's path; X_0 is a standard air mass, or optical depth, calculated for a vertical path to the zenith above sea level; and b is

the extinction coefficient. Astronomers usually rewrite the Lambert–Beer law in terms of stellar magnitudes, in which form it is known as Bouguer's law:

$$m - m_0 \equiv 2.5[\log_{10}(I_0) - \log_{10}(I)] = kX/X_0, \quad (10)$$

where

$$k \equiv 2.5 \log_{10}(e)b = 1.08574b \quad (11)$$

is the extinction coefficient if expressed on the stellar magnitude scale. For an idealized Rayleigh atmosphere, $k = 0.1054$ for visible light of $\lambda = 550$ nm. Mie scattering by aerosols and absorption, mostly by ozone, increases the extinction and at sea level, a value of $k \approx 0.25$ is more typical [10]. From a survey of different observatories [11], $k \approx 0.15$ seems appropriate for circumstances of very good visibility [12–15]. We will adopt this value for our analysis and discuss the consequences of our choice at the end of the next subsection.

D. Results

Figure 7 shows how the relative air mass varies with the observed altitude within the ensemble of the about 20,000 rays that have suffered one single reflection for an aircraft at flight level 12 km looking at a cloud of crystals between 1.5 and 14 km in height. All conceivable solar heights resulting in a halo point of the super/subsun between altitude -15° and the mirror horizon cutoff of $+3^\circ.3$ are considered. The subsun is seen to have its strongest extinction on the apparent horizon, at $-3^\circ.3$. The most prominent feature of Fig. 7 is, however, the extremely strong angle dependence for the supersun, which shows a deep minimum, and thus a minimal extinction, right on the true horizon.

The radiance distribution as calculated for the situation under study is shown in Fig. 8. The sun is at $-3^\circ.2$, just above the apparent horizon. The distribution has two maxima, separated by a minimum around an altitude of 1° . This minimum

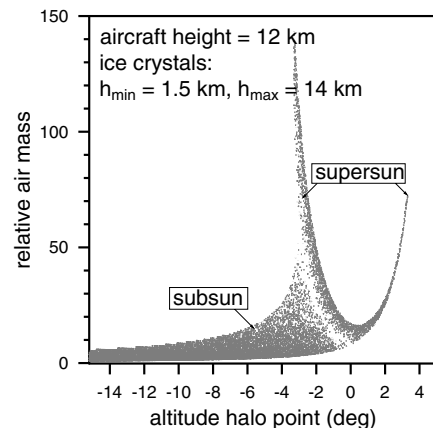


Fig. 7. Relative air mass X/X_0 for the calculated single-reflection ensemble of ray tracings, which contribute to the formation of the subsun or the supersun. Halo points of the subsun or supersun have been calculated between altitude -15° and $+15^\circ$, but the mirror horizon imposes a cutoff at $3^\circ 19'$.

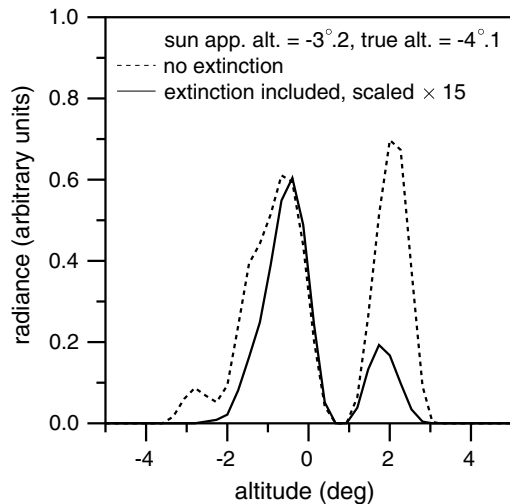


Fig. 8. Radiance distribution of the supersun as a function of altitude, as seen from a flight level of 12 km, with the sun just above the $3^{\circ}.3$ dipped apparent horizon. The dashed line neglects atmospheric extinction, while for the $15\times$ scaled-up solid line it is included.

is due to the fact that here the reflection locus rises until above 14 km, which was adopted as an upper limit for the ice crystals. The introduction of an upper boundary lower than the locus's top eliminates a segment of the supersun centered just above the aircraft's true horizon (see the second special point of Table 1). This effect is also apparent from Fig. 6, where near altitude $\sim 1^{\circ}$, the vertical line drawn at $3^{\circ}.2$ passes through a region void of dots. Extinction is seen to reduce the above-horizon peak (centered at altitude $+2^{\circ}$) much stronger than the subhorizon one (centered at -2°), because the latter is closer to the true horizon (0°). Thus, while geometrically the supersun should range from $-3^{\circ}.2$ to $+3^{\circ}.2$, its brightness is mainly concentrated in a relatively narrow region, just below the true horizon. This agrees remarkably well with the observation of an elongated spot, extending from $1^{\circ}.8$ to $2^{\circ}.6$ above the sun's upper limb (see Section 1).

Figure 9 presents the radiance distributions for different sun heights in a way similar to Fig. 6. As mentioned earlier, the inclusion of atmospheric refraction leaves the global geometric features largely unchanged. The calculated brightness distributions in Fig. 9 have been obtained by a horizontal binning

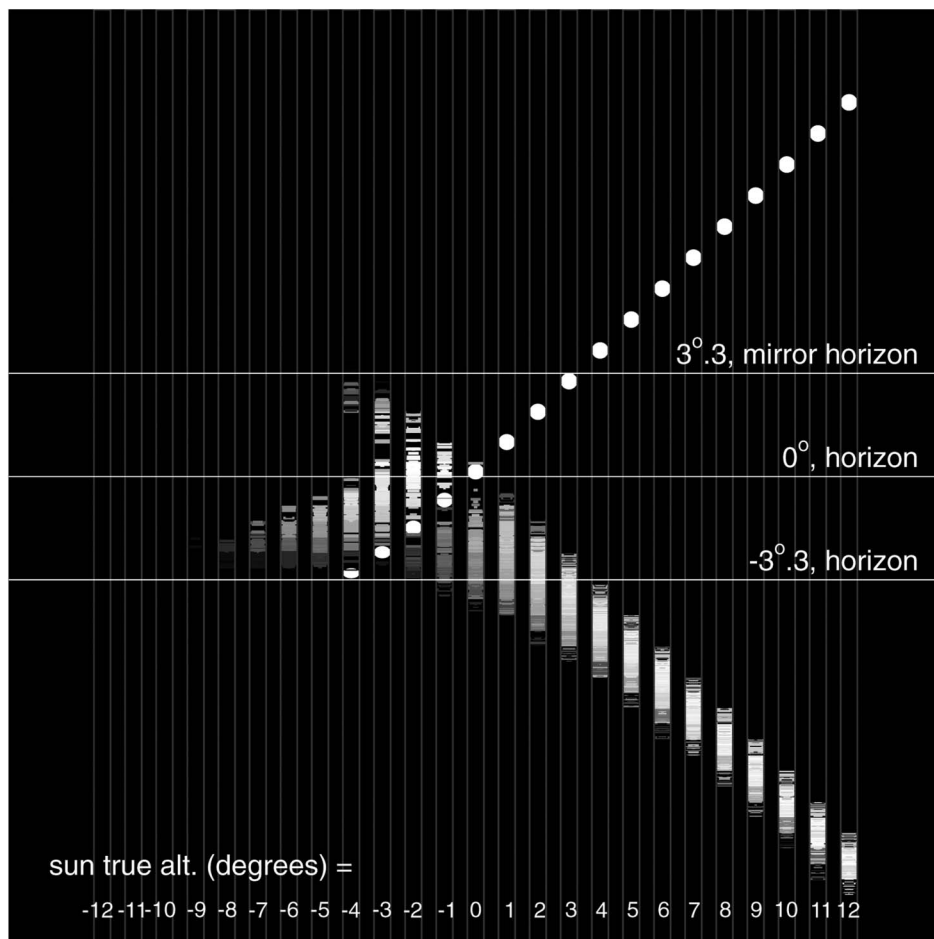


Fig. 9. Transition of the subsun into the supersun, as seen from a flight level of 12 km, in the presence of ice crystals between 1.5 and 14 km above the Earth. The brightness of the subsun/supersun in the drawing is represented on a logarithmic scale, spanning a difference of 10 stellar magnitudes between white and black. An extinction coefficient $k = 0.15$ has been adopted.

in intervals, equal in width to the sun's diameter, 32'. Radiance is visualized by a gray value, $\text{rgb255}(g, g, g)$, where g is taken proportional to the calculated (stellar) magnitude [Eq. (10)]. The maximum radiance in the simulation is associated with $g = 255$ (white) and 0 (black) is made to correspond to a lower radiance, different from the maximum by 10 stellar magnitudes. The maximum radiance encountered in the subsun region is much larger than that in the supersun region. For reasons of presentation, we have therefore done this "gray tone calibration" in both regimes separately, assigning in each of them white to their maximum brightness and black to a brightness that is 10 stellar magnitudes lower.

Besides being convenient, the presentation of radiances on a logarithmic scale is justified by Fechner's law [16], which states that we perceive the intensity of stimuli on a logarithmic rather than a linear scale.

For the presentation of Fig. 9, we have chosen an extinction coefficient $k = 0.15$ and a span of 10 in stellar magnitude between white and black. Might someone find this k value too small, then he may imagine the figure to have been made for a higher k , with the span in magnitude increased accordingly.

We acknowledge that our computer simulations will never be able to give a full match with the radiance distribution of the observed feature (Fig. 1) because the extinction by clouds in the frontal systems and its blocking of incoming light to the crystals cannot be modeled. Nevertheless, quantitative agreement between observation and calculation emerges, which provides some confidence in the interpretation of Fig. 1 being indeed a picture of the supersun.

4. Discussion and Conclusion

A. Conditions for Observing the Supersun

A supersun above the setting sun may also be visible from heights lower than the aircraft's cruise height. The primary condition for its formation is that the sun must be below the true horizon. With the sun at the apparent horizon, the full extension range of the supersun equals twice the value of the horizon dip. So for a mountain-based observer (1000 m), the maximum length of the supersun is $1^\circ.9$, while for a tower-based observer (100 m) $0^\circ.6$ and for an observer standing on a dune near the beach (10 m), it is $0^\circ.2$. An observer standing at ground level will never see the supersun, as the light path sun-crystal will always be blocked by the surface of the Earth.

These above-mentioned ranges are the geometrical limits of the length of the supersun. Within these ranges, extinction in the total light path is minimal for halo points appearing at the true horizon, so that even for fully developed supersuns, a maximum in brightness will appear in a region around altitude 0° .

Full development of the supersun requires that the observer is surrounded by crystals, that the sun is about to set, and that the crystal layer reaches higher

than the maximal height of the locus of reflecting crystals (second special point of Table 1). For mountain-based observers, the first and last requirements are easier fulfilled than for high-flying jets, so mountaineers may more often encounter a fully developed supersun. For near-ground-based or tower-based observers living outside the polar regions, the observation will be much rarer, as even in winter time they will only very rarely be surrounded by crystals. However, tower-based observers living in cold climates may occasionally encounter this feature in full development.

B. Supersun Versus Pillar

Imperfectness in the orientation of the plate-orientation increases the length of the supersun: a dispersion of, e.g., 1° in the tilt angle of the crystals causes it to extend to 2° above the supersolar point. This is easily verified by our ray-tracing program when a wobble in the crystal's orientation is added via a random Gaussian variable. This result implies that the mirror horizon no longer cuts off the supersun from above. Seen from an aircraft, the 2° stretch of the supersun is, however, still small compared to its length, which under idealized conditions is 6° . The resulting phenomenon can still be regarded as a stretched supersun. However, seen from a tower from which the supersun's length is only $0^\circ.6$, a plate orientation that is tenfold better is needed to keep the supersun at the same level of recognizability as from an aircraft. Hence, the larger the wobble of the crystals or the lower the observer's altitude, the more the supersun is stretched relative to its length under idealized conditions and the less its typical features can be recognized. At some stage, one would be inclined to call the phenomenon a pillar; this happens when the effect of the Earth's curvature on the shape of the feature starts to become small relative to the effect of imperfections in the crystal orientation. In fact, the distinction between the supersun and the pillar is not sharp but it is a sliding scale, based on the degree of perfection in the orientation of the ice crystals.

It may be useful to set, for the phenomenon above the sun, the criterion that distinguishes the supersun from a pillar as sharp as possible. We propose to reserve the name pillar for the part of the halo that is seen above the mirror horizon. This criterion is consistent with the most common notion of a pillar: for an observer on the ground, horizon and mirror horizon coincide and a light pillar that he might see above the setting or subhorizon sun is entirely due to imperfectly oriented crystals. In the same way, when the observation is made from an elevated position, the part of the halo above the mirror horizon should be called a pillar. The part between the horizon and mirror horizon does not require imperfectly oriented crystals to exist. In its idealized form, as caused by perfectly oriented crystals, we have named the phenomenon above the sun but below the mirror horizon the supersun, and we continue to use this

name also when a dispersion in the crystal's orientations produces a pillar above it.

C. Relation with the Parhelic Circle

There exists a similarity between the supersun and the parhelic circle, in the sense that the supersun can be regarded as a segment of a rotated parhelic circle—one that passes through sun and zenith [17]. Both halo forms can be ascribed to reflecting crystal faces that have a freedom to rotate about a fixed axis in space: vertical for the parhelic circle, horizontal and perpendicular to the plane sun–zenith–observer for the supersun. The difference is that the degree of freedom to rotate is restricted in the case of the supersun so that only a short segment of this “vertical parhelic circle” shows up.

D. Deformation of Other Halos

The curvature of the Earth may affect the shapes or positions of halos other than the subsun, among them the parhelia and the subparhelion. Near-horizon parhelia formed in high clouds may even for ground-based observers show a downward displacement of maximally $0^{\circ}.2$ —small, but perhaps perceivable if the parhelion appears above a well-defined horizon, e.g., over the sea. A subparhelion, on the other hand, would strongly deform into a feature similar to the supersun: for an elevated observer and the sun below the true horizon, it transforms into a vertical band at 22° left or right from the sun, extending from the (dipped) apparent horizon to the mirror horizon. Reports of this phenomenon are lacking, although a recent picture by Hinz [18] taken at a sun altitude of $-1^{\circ}.8$ from the top of the 1835 m Mount Wendelstein contains a possible hint of it.

The authors thank Piet Stammes, Jan Willem Pel, and Sergey Kivalov for many discussions on the topic of atmospheric extinction.

References and Notes

1. L. Cowley and M. Schroeder, HaloSim3 Software, <http://www.atoptics.co.uk/halo/halfeat.htm>.
2. W. Tape and G. P. Können, “A general setting for halo theory,” *Appl. Opt.* **38**, 1552–1625 (1999).
3. G. P. Können, “Symmetry in halo displays and symmetry in halo-making crystals,” *Appl. Opt.* **42**, 318–331 (2003).
4. In German the subsun is known as the “Untersonne,” and “Übersonne” would be the appropriate translation for supersun. In French, the “sub-soleil” or “soleil inferieur” would find their logical counterparts in “super-soleil” and “soleil superieur.” In Dutch the subsun is called “onderzon” and the supersun will be the “bovenzon.”
5. S. Y. van der Werf, “Ray tracing and refraction in the modified US1976 atmosphere,” *Appl. Opt.* **42**, 354–366 (2003).
6. S. Y. van der Werf, G. P. Können, and W. H. Lehn, “Novaya Zemlya effect and sunsets,” *Appl. Opt.* **42**, 367–378 (2003).
7. S. Y. van der Werf, “Comment on ‘Improved ray tracing air mass numbers model,’” *Appl. Opt.* **47**, 153–156 (2008).
8. D. R. Lide, *Handbook of Chemistry and Physics*, 81st ed. (CRC, 2000).
9. W. Tape, *Atmospheric Halos*, Antarctic Research Series (American Geophysical Union, 1994), Vol. 64.
10. Astronomical observatories often document values of k per amount of air mass relative to their own unit air mass above the site of the observatory, X_{obs} , instead of the unit air mass at sea level, X_0 . This must be kept in mind when comparing extinction parameters for different observatories.
11. A. Meinel and M. Meinel, *Sunsets, Twilights and Evening Skies* (Cambridge University, 1983).
12. H. Tüg, “Measurements of the energy distributions of southern standard stars from 3200 Å to 8800 Å,” *Astron. Astrophys.* **82**, 195–202 (1980).
13. M. Golay, *Introduction to Astronomical Photometry* (Reidel, 1974).
14. V. B. Nikonov, “Methods of Investigating Variable Stars,” (NASA Technical Translation TT-F-797, Washington, 1973).
15. P. Wang, W. H. Knap, P. Kuipers Munneke, and P. Stammes, “Clear-sky shortwave radiative closure for the Cabauw Baseline Surface Radiation Network site, the Netherlands,” *J. Geophys. Res.* **114**, D14206 (2009).
16. G. T. Fechner, *Elemente der Psychophysik* (Breidkopf und Härtel, 1860), Vol. II, Chap. 16, English translation from the 1912 edition, <http://psychclassics.yorku.ca/Fechner/>.
17. K. Hariti, “Parhelic circle over the Dead Sea,” *Atmospheric Optics* (2007), <http://www.atoptics.co.uk/halo/parcirc.htm>.
18. C. Hinz, “Upper parhelia over the Alps,” *Ice Crystal Halos* (2010), http://www.ursa.fi/blogit/ice_crystal_halos/index.php?title=upper_parahelia_over_the_alps.